Journal of Solid State Chemistry 184 (2011) 3002–3007

Contents lists available at SciVerse ScienceDirect

Journal of Solid State Chemistry

journal homepage: www.elsevier.com/locate/jssc

Boron and nitrogen-codoped TiO_2 nanorods: Synthesis, characterization, and photoelectrochemical properties

Xiaosong Zhou [a,b], Feng Peng [a,*], Hongjuan Wang [a], Hao Yu [a]

[a] School of Chemistry and Chemical Engineering, South China University of Technology, Guangzhou 510640, PR China
[b] School of Chemistry and Technology, Zhanjiang Normal University, Zhanjiang 524048, PR China

ARTICLE INFO

Article history:
Received 26 April 2011
Received in revised form
17 August 2011
Accepted 14 September 2011
Available online 17 September 2011

Keywords:
Photocatalyst
Boron and nitrogen codoped TiO_2
Nanorods
Photoelectrochemical property

ABSTRACT

Boron and nitrogen codoped TiO_2 nanorods (BNTRs) were synthesized via two-step hydrothermal reactions using TiN as a starting material. The as-prepared samples were characterized by X-ray diffraction, field-emission scanning electron microscope (SEM), transmission electron microscopy and X-ray photoelectron spectroscopy techniques. The results showed that TiO_2 nanorods with the diameter of approximately 50–100 nm and the length of several micrometers were doped by the interstitial N and B. The nanorods were firstly formed in the hydrothermal synthesis of nitrogen doped TiO_2. The growing process of nanorods was observed by SEM and a most probable formation mechanism of the trititanate nanorods was proposed. The BNTRs showed a higher photocatalytic activity and a bigger photocurrent response than N–TiO_2 nanorods under visible light irradiation.

1. Introduction

Nanostructure titania materials have attracted enormous interest owing to their extensive applications in catalysts, electronic and photonic devices, gas sensors, solar cells and bio-medical components [1–6]. Various forms of titania, such as nanopowders [1], nanotubes [7], nanorods [8], fibers [9], whisker [10] and mesoporous materials [11], have been reported. One-dimensional (1D) titania nanomaterials, especially titania nanorods, have become the focus of current research on nanotechnology. Many techniques have been reported to synthesize one-dimensional TiO_2 nanorods. For example, Uhm et al. [12] prepared anatase- and rutile-phase N–TiO_2 nanorods *via* decomposition of gas-phase titanium tetrachloride ($TiCl_4$) by an atmospheric microwave plasma torch, based on the conventional vapor–liquid–solid growth mechanism. Zhao et al. [13] synthesized highly ordered TiO_2 single-crystalline nanorod/nanotube arrays by directly anodizing a modified titanium foil. Compared with the nanotube arrays prepared by photoanode, these ordered arrays exhibited unique feature of selective photocatalytic oxidation of water and glucose. Lokhande et al. [14] prepared TiO_2 nanorods on glass substrate using soft chemical route at room temperature, which were treated with electron beam irradiation after annealing. The result showed that the electron bombardment made amorphous structure into the crystalline, and increased the length and the diameter of the nanorods. Shao et al. [15] synthesized fluorine-doped rutile titania nanorods and thin films using a hydrothermal method. The results showed that the substitution of ethanol for water as a solvent was highly effective in promoting the one-dimensional growth of the rutile nanorods and increasing their packing density in the thin films. Recently, the B,N-codoped titania has been considered as the most effective approach to improve photocatalytic activity in visible region [16]. However, to our knowledge, no report about the fabrication of the boron and nitrogen codoped TiO_2 nanorods has been published.

Herein, we designed and synthesized successfully the novel boron and nitrogen codoped TiO_2 nanorods (BNTRs) by hydrothermal method. The photocatalytic activity of as-prepared samples was studied based on methyl orange dye (MO) degradation. The photoelectrochemical performance was evaluated based on photocurrent response. The results demonstrated that the BNTRs exhibited a higher photocatalytic activity and a bigger photocurrent response than NTRs under visible light irradiation.

2. Experimental

2.1. Samples preparation

In a typical synthesis, 500 mg TiN (Hefei Kaier Nano Company (China)) was added into 80 mL NaOH aqueous solution (10 M). The mixture was stirred for 1 h and then transferred into a 100 mL Teflon-lined stainless steel autoclave. The autoclave was sealed and put into a preheated oven to perform hydrothermal treatment at 200 °C for 12 h. After hydrothermal processing,

* Corresponding author. Fax: +86 20 87114916.
E-mail address: cefpeng@scut.edu.cn (F. Peng).

0022-4596/$ - see front matter © 2011 Elsevier Inc. All rights reserved.
doi:10.1016/j.jssc.2011.09.017

the gray fluffy power was collected and washed with copious amounts of distilled water and 0.1 M hydrochloric acid until the pH of the washing solution was less than 7. This product was then dried in air at 60 °C for 24 h to obtain the N–TiO_2 nanorods. The samples were then added to 80 mL of 1 M H_3BO_3 and stirred for 30 min. Then the mixture was transferred to a 100 mL Teflon-lined stainless steel autoclave again and heated at 200 °C for 24 h. The precipitate was collected and washed with distilled water and absolute alcohol three times, and then dried in air at 80 °C overnight. The samples were then heated in a quartz tube furnace at different temperatures' range from 400 °C to 600 °C for 2 h at a ramp rate of 1 °C/min to obtain the B,N–TiO_2 nanorods that was denoted as BNTRs-*T* (*T* denotes annealed temperature). The N–TiO_2 nanorods were also annealed at 550 °C for 2 h in ambient air for comparison, and were denoted as NTRs-550.

2.2. Sample characterizations

The crystal structure of samples was characterized by powder X-ray diffraction (XRD) (D/max-IIIA, Japan) using Cu *K*α radiation. The morphology was observed with a field-emission scanning electron microscopy (SEM) (LEO1530VP, LEO Company) and transmission electron microscopy (TEM, JEOL, JEM2010). The UV–vis absorption spectra were measured with a Hitachi UV-3010 spectrophotometer equipped with an integrating sphere assembly and using the diffuse reflection method and $BaSO_4$ as a reference. The Brunauer–Emmett–Teller (BET) surface area (S_{BET}) was determined by nitrogen adsorption–desorption isotherm measurements at 77 K on a Micromeritics ASAP 2010 system. The samples were degassed at 473 K until a pressure lower than 10^{-6} Torr is obtained before the actual measurements. The X-ray photoelectron spectroscopy (XPS) was performed on the titania nanorods with Krato Axis Ultra DLD spectrometer (Al *K*α X-ray, $h\nu = 1486.6$ eV). The binding energy (BE) of the XPS spectra was calibrated with the reference of C 1*s* peak at 284.6 eV.

2.3. Photocatalytic reaction

The photocatalytic reaction was conducted in a 200 mL cylindrical glass vessel fixed in the XPA-II photochemical reactor (Nanjing Xujiang Machine-electronic Plant). A 500 W Xe lamp was used as the simulated solar light source (UV–vis light), and a house-made filter was mounted on the lamp to eliminate infrared irradiation. The visible light was obtained using the cut-off filter. The cut-off filter was made up of 1 M sodium nitrite solution, which can absorb the light with wavelength under 400 nm [17]. Methyl orange dye (MO) with the concentration of 20 mg/L was used as contamination. In order to obtain an optimally dispersed system and reach complete adsorption/desorption equilibration, 50 mg photocatalyst powder was dispersed in 200 mL reaction solutions by ultrasonicating for 15 min and then the suspension was magnetically stirred in dark for 1 h. During the photocatalytic reaction, air was blown into the reaction medium at a flow rate of 200 mL/min. At regular intervals, 8 mL of the suspension was filtered and then centrifuged. The concentration of the remaining MO was measured by its absorbance (*A*) at 465 nm with a Hitachi UV-3010 spectrophotometer. The decolorization ratio of MO could be calculated by $(A_0 - A)/A_0 \times 100\%$.

2.4. Photocurrent measurements

To prepare the working electrodes, 500 mg of the hydrothermal treated NTRs or BNTRs samples (without calcination) was first dispersed into a mixture of 2.0 mL ethanol and 0.1 mL terpinol and sonicated for 30 min to form a slurry, then the resulting slurry was coated on FTO glass (2.3 mm, 15 Ω/square, Nippon Sheet Glass, Japan) using a screen-printing method. The TiO_2 film thickness is dependent on the repeating times of the screen printing process. The TiO_2 films were sintered at 500 °C for 30 min in air. The photocurrents were measured using a standard three electrodes photoelectrochemical cell, which was carried out by an electrochemical workstation (CV-27, BAS). The as-prepared photocatalysts, platinum-gauze and Ag/AgCl and were used as working, counter and reference electrodes, respectively. A sodium sulfate solution (1 M) was used as electrolyte. The chopped (≈ 0.25 Hz) light for the photocurrent was the filtered light ($\lambda > 400$ nm, 150 mW/cm^2) from a PLS-SXE300UV Xe lamp (Changtuo, Beijing).

3. Results and discussion

Fig. 1 shows XRD patterns of the BNTRs at different annealing temperatures. The diffraction peaks can be assigned to anatase (JAPDS no. 84-1286) [18] and rutile (JAPDS no. 78-1509) [19] with preferential reflections of (101) for anatase and (110) for rutile, respectively. With the increasing annealing temperature, the peak intensities of anatase phase decrease and those of rutile phase increase accordingly, which indicates that anatase phase transforms to rutile phase.

Raman spectra were applied as an additional tool to probe the phase formation of BNTRs, shown in Fig. 2. There are five typical active modes of anatase TiO_2: Eg (144 cm^{-1}), Eg (200 cm^{-1}), B1g (399 cm^{-1}), A1g (518 cm^{-1}), Eg (639cm^{-1}) and four typical active modes of rutile TiO_2: B1g (143 cm^{-1}), Eg (240 cm^{-1}), Eg (447 cm^{-1}), A1g (612 cm^{-1}), in BNTRs. Compared with the reference anatase [20] and rutile [21] TiO_2, the as-prepared samples show the shift of Eg mode (200 cm^{-1}) and A1g mode (518 cm^{-1}) for anatase TiO_2 toward higher wave numbers by 3 cm, and the shift of Eg mode (240 cm^{-1}) for rutile TiO_2 toward higher wave numbers by 5 cm. These shifts imply the possible formation of the Ti–O–N and Ti–O–N–B structures on the surface of BNTRs [22,23]. These surface structures formed on TiO_2 would inevitably impair the symmetry of Ti–O–Ti network and thus change some force constants, which intrinsically determine the wave number of corresponding active Raman modes. Liu et al. [24] have reported that the replacement of iodine atom for titanium atom also led to the similar shift of Eg mode at 144–149 cm^{-1}. It is obvious that the intensities of rutile modes increase with the

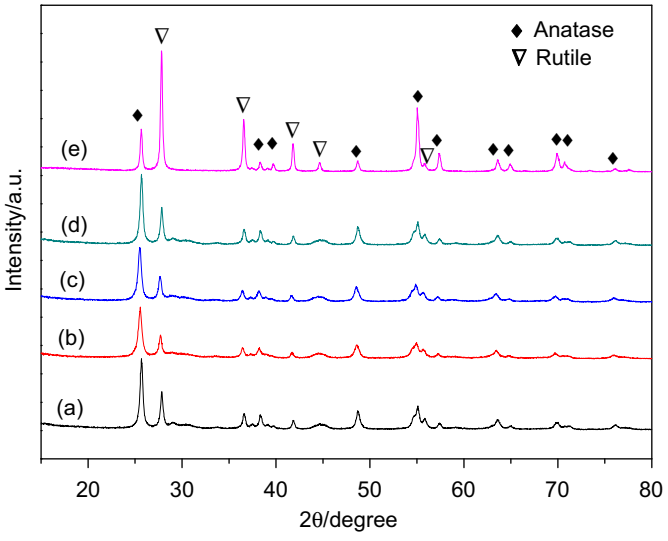

Fig. 1. XRD patterns of NTRs and BNTRs: (a) NTRs-550; (b) BNTRs-450; (c) BNTRs-500; (d) BNTRs-550; and (e) BNTRs-600.

annealing temperature increasing from 450 °C (BNTRs-450) to 600 °C (BNTRs-600), which suggests the transformation from anatase phase to rutile phase. This result agreed well with the XRD results.

Fig. 3a and b reveals the SEM and the TEM images of NTRs-550. The average diameter of the nanorods is approximately 50–100 nm and the length is several micrometers. The surface of the nanorods is very clear and glazed. After hydrothermal treatment in H_3BO_3 solution, the surface of nanorods was eroded seriously, and some nanorods were cut off to several hundred nanometers in length, as shown in Fig. 3c and d. The BET surface area of BNTRs-550 (38.94 m^2/g) is a little higher than that of NTRs-550 (34.43 m^2/g) (shown in Table 1), which is more propitious for a catalyst.

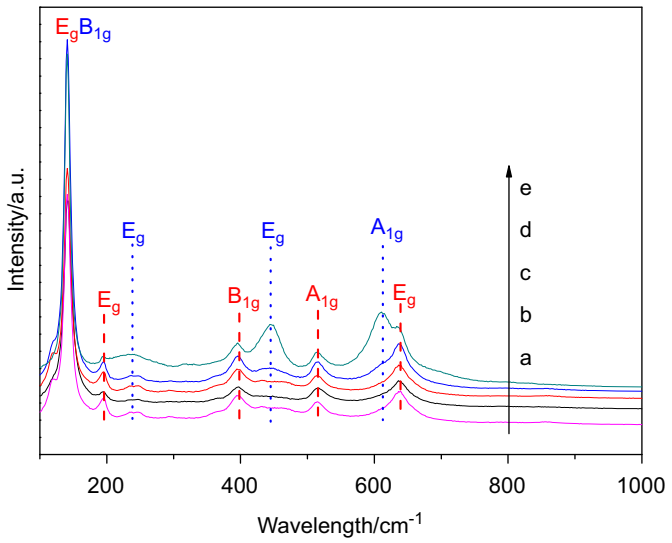

Fig. 2. Raman patterns of NTRs and BNTRs: (a) NTRs-550; (b) BNTRs-450; (c) BNTRs-500; (d) BNTRs-550; and (e) BNTRs-600.

Based on the above results, it is clear that the nanorods were firstly formed in the hydrothermal synthesis of nitrogen doped TiO_2. A most probable formation mechanism of the trititanate nanorods is elucidated based on the SEM pictures at different synthesis stages, as shown in Scheme 1. At the very early stage, there were TiN, NaOH, H_2O and a little air in the autoclave (Scheme 1a). Under hydrothermal condition, pressure was formed, and then TiN dissolved into solution and began to react with NaOH and O_2 in solution to form a highly disordered intermediate phase trititanate (expressed as $Ti_3N_xO_{7-x}^{2-}$) containing Ti, O, N and Na (Scheme 1b). When such trititanate nanoclusters became supersaturated, they began to crystallize as $Na_xTiN_yO_z$ nanorods (Scheme 1c). These nanorods continue to grow in the length with the reaction time. After being washed by hydrochloric acid and thermally treated, the N–TiO_2 nanorods were formed (Scheme 1d). Hu et al. [25] also reported that the preferential one-dimensional growth occurred in the presence of reactants as long as the catalyst (Ti species in our experiment) remained in the liquid. When the NTRs were hydrothermally treated in H_3BO_3 solution, the NTRs were eroded seriously by H_3BO_3 and doped by boron to form the uneven BNTRs.

The chemical states of nitrogen and boron on the surfaces of NTRs-550 and BNTRs-550 were investigated with high-resolution XPS, as shown in Fig. 4. The peak positions of N, B, O and Ti and the contents of boron and nitrogen and are summarized in Table 1. From the N 1*s* spectra of NTRs-550 and BNTRs-550 in Fig. 4a, it can be seen that there is a peak located at around 399.1 eV for both the samples and there is a new peak appearing at 397.7 eV for BNTRs-550. Based on the earlier reports [26–28], we can assign the N 1*s* peak at around 399 eV to oxidized nitrogen in the form of O–N linkages in interstitial nitrogen. The other N 1*s* peak at 397.7 eV can be attributed to Ti–O–N–B [22,23]. The N content of BNTRs-550 (0.79%) is lower than that of NTRs-550 (1.03%), which indicates that there is some N loss during the B doping procedure. For the B 1*s* spectra of the BNTRs-550 in Fig. 4b, there is only one peak at 190.0 eV, which is originated from Ti–O–N–B [22,23]. In Fig. 4c, for both NTRs-550 and BNTRs-550, the core level peaks

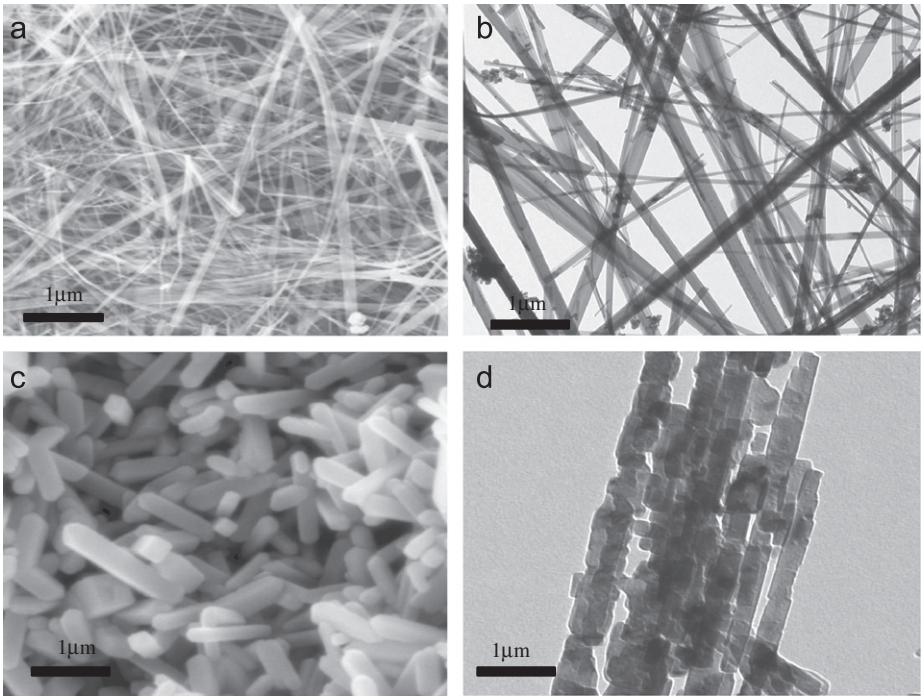

Fig. 3. SEM (a, c) and TEM (b, d) photos of as-prepared samples: (a) and (b) NTRs-550; (c) and (d) BNTRs-550.

Table 1
XPS peak positions and element contents of NTRs-550 and BNTRs-550.

Samples	B (at%)	N (at%)	B 1*s* (eV)	N 1*s* (eV)	O 1*s* (eV)	Ti 2*p* (eV)	S_{BET} (m^2/g)
NTRs-550	–	1.03	–	399.1	531.7, 530.0	463.7, 458.0 462.6, 456.5	34.43
BNTRs-550	0.63	0.79	190.0	399.2, 397.7	532.0, 530.0	463.7, 458.0	38.94

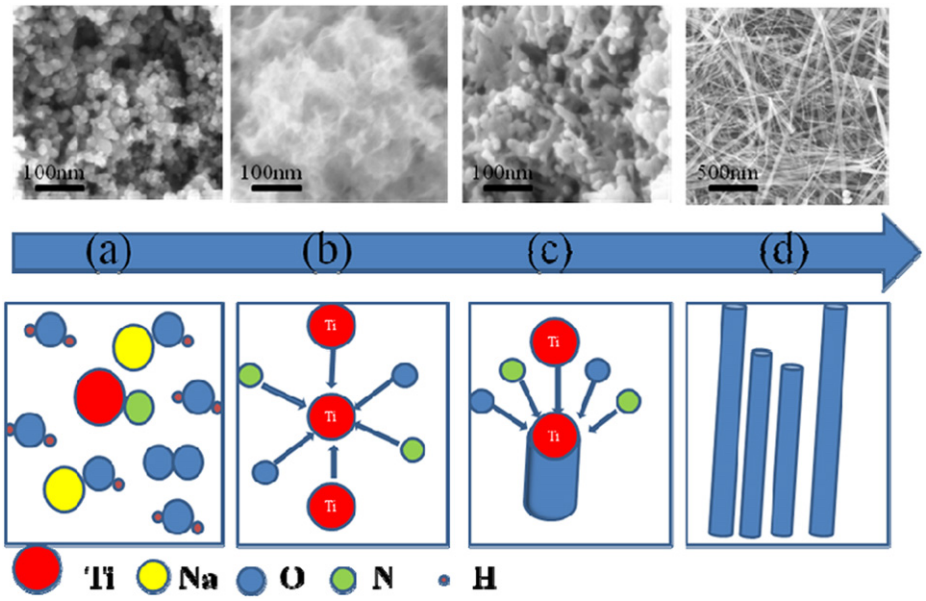

Scheme 1. Proposed NTRs' growth process and corresponding SEM photos: (a) TiN; (b) after reaction 0.5 h; (c) after reaction 1 h; and (d) after reaction 12 h.

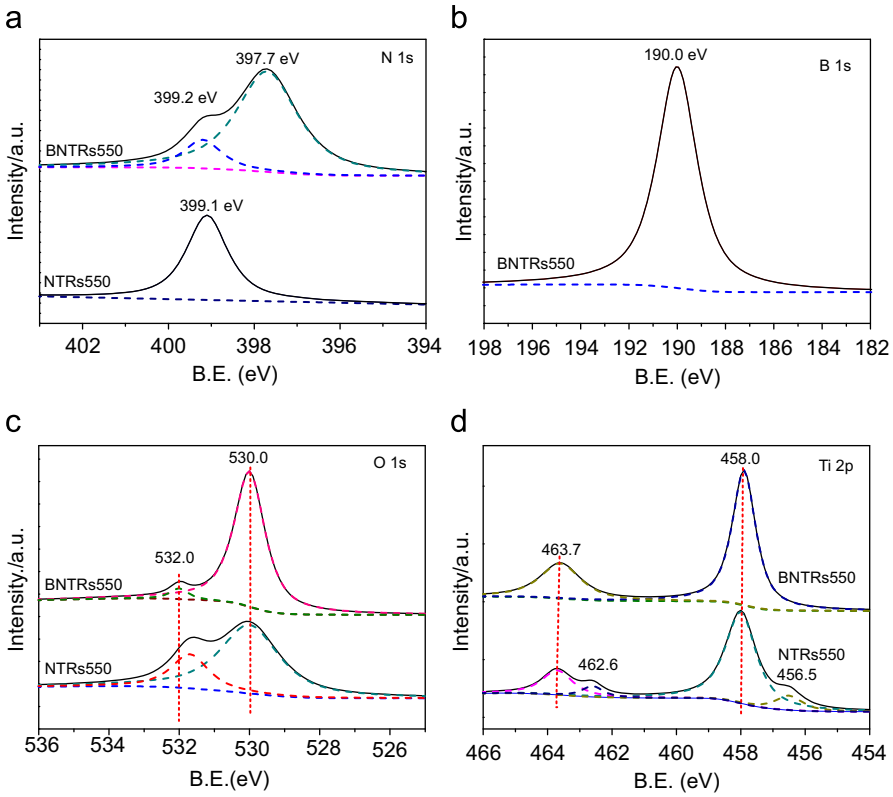

Fig. 4. XPS spectra of samples NTRs-550 and BNTRs-550: (a) N 1*s*; (b) B 1*s*; (c)O 1*s*; and (d) Ti 2*p*.

of O 1*s* appear at about 530.0 eV and 532.0 eV. The peak of O 1*s* at about 530.0 eV comes from Ti–O–Ti linkages in TiO_2 [29,30]. We attribute the O 1*s* peak at about 532.0 eV to O–N–B linkages in BNTRs-550 [21,22] and O–N linkages in NTRs-550 [26–28]. The main pair of peaks of Ti $2p_{3/2}$ and $2p_{1/2}$ for NTRs-550 and BNTRs-550 appear at 458.0 and 463.7 eV, respectively (Fig. 4d), which can be

assigned to Ti^{4+} 2*p* peaks. As a rule, the Ti^{4+} $2p_{3/2}$ and $2p_{1/2}$ peaks appear at 458.9 and 464.7 eV in pure TiO_2 [29,31]. Most of the reports agreed on the lower B.E. of Ti 2*p* in doped TiO_2 [29,31], and they attribute the lower shift of Ti *2p* to the replacement of higher electro-negative oxygen by lower electro-negative nitrogen. The main pair of peaks of Ti $2p_{3/2}$ and $2p_{1/2}$ for NTRs-550 and BNTRs-550 shift to the lower B.E. by 0.9 and 1.0 eV compared with pure TiO_2, which suggests the successful incorporation of nitrogen or boron into the TiO_2 lattice. However, the NTRs-550 has another pair of Ti $2p_{3/2}$ and $2p_{1/2}$ peaks at 456.5 and 462.6 eV, respectively, which can be attributed to N–Ti linkages from the original material of TiN [32]. While this pair of Ti 2*p* peaks disappear in BNTRs-550, indicating that TiN was oxidized completely after H_3BO_3 solution hydrothermal treatment. From XPS data, it is clear to see the formation of Ti–O–N–B structures in BNTRs-550.

Fig. 5 gives the UV–vis absorption spectra of the as-prepared NTRs-550 and BNTRs samples. It can be seen clearly that there is a strong visible light absorption from 400 nm to 550 nm for the as-prepared samples. However, the visible light absorption of BNTRs becomes weaker and weaker with the increase of annealing temperature, suggesting that annealing temperature has great effect on the UV–vis absorption of the BNTRs.

Fig. 6 shows the photocatalytic activity of the as-prepared samples in degrading organic pollutant MO under visible light irradiation. The photolysis performance of MO is also shown in Fig. 6a; the decolorization ratio is only 5.5% after 2.5 h irradiation, which shows that MO is less degraded under visible light irradiation without catalyst. The photocatalytic decolorization ratio of MO by NTRs-550 is 36.1% after 2.5 h visible light irradiation. However, to BNTRs samples, the decolorization ratio of MO is drastically improved. The decolorization ratio of MO increases first and then decreases with the increase of annealing temperature, which indicates that annealing temperature affects the photocatalytic activity of BNRTs. The highest decolorization ratio of MO reaches 94.5% with BNTRs-550, which is more than 2.5 times than with NTRs-550. So, with the B and N co-doping, an improved visible light photocatalytic activity is observed.

The photocurrent response measurement was carried out under visible light irradiation to investigate the photo-induced charges separation efficiency of NTRs and BNTRs, as shown in Fig. 7. It can be seen that photocurrent of BNTRs (366.29 $\mu A/cm^2$) is three times than that of NTRs (120.52 $\mu A/cm^2$). Higher photocurrent means that more photo-induced electrons can transfer from BNTRs to counter electrode via external circuit, under the visible light illumination, and then lead to higher photocatalytic activity. So the higher photocurrent of BNTRs is in good agreement with the higher photocatalytic activity. The photocatalytic activity and photocurrent response of BNTRs is superior to those of NTRs, which indicates that the BNRTs with B and N co-doping are more suitable to be used as photocatalyst than NTRs.

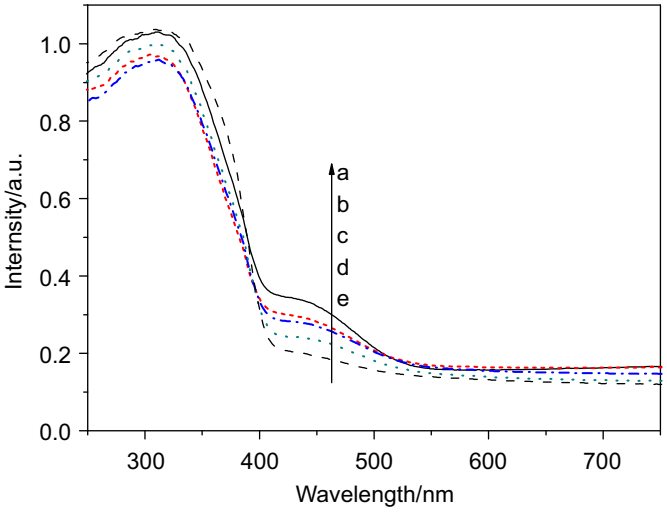

Fig. 5. UV–vis absorption spectra of samples: (a) BNTRs-450; (b) BNTRs-500; (c) BNTRs-550; (d) BNTRs-600; and (e) NTRs-550.

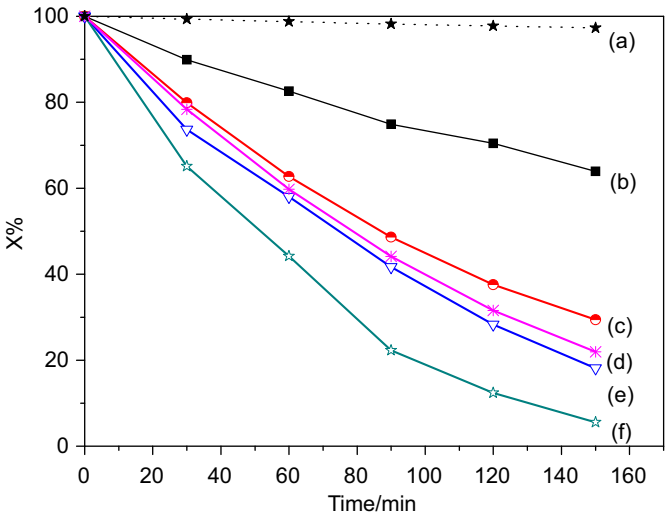

Fig. 6. Photocatalytic degradation ratios of MO under visible light: (a) no catalyst; (b) NTRs-550; (c) BNTRs-450; (d) BNTRs-500; (e) BNTRs-600; and (f) BNTRs-550.

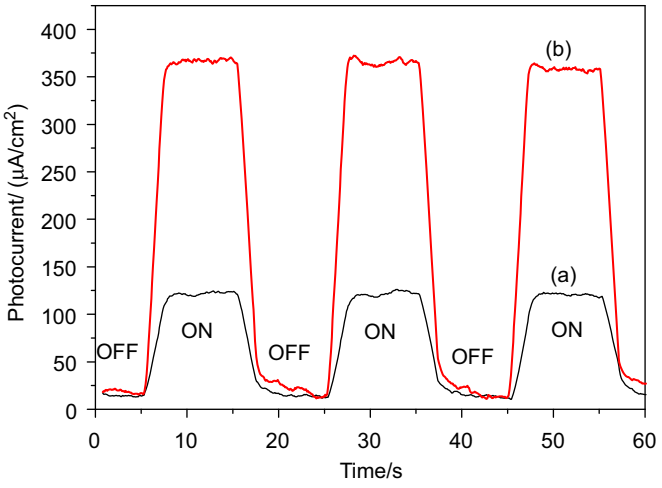

Fig. 7. Photocurrent responses of: (a) NTRs and (b) BNTRs.

4. Conclusions

The BNTRs were prepared using TiN as precursor by the two-step hydrothermal method. The SEM and TEM pictures show that the diameter of the nanorods is approximately 50–100 nm and the length reaches to several micrometers. The nanorods were firstly formed in the hydrothermal synthesis of nitrogen doped TiO_2, and a most probable formation mechanism of the trititanate nanorods was proposed. The XPS results suggested that boron and nitrogen are located into the TiO_2 lattice interstitially. With B and N doping, an improved visible light photocatalytic activity is observed. The average photocurrent density of the BNTRs is three times than that of the NTRs under visible light irradiation. The BNTRs developed in this paper will be potentially promising solar energy materials for solar cells and organic pollutant degradation.

Acknowledgment

The authors thank the National Natural Science Foundation of China (no. 20873044) and the New Century Excellent Talents in University of China (NCET-08-0205) for financial support.

References

[1] H.Y. Lee, G.M. Kale, Int. J. Appl. Ceram. Technol. 5 (2008) 657.
[2] X.F. Duan, Y. Huang, Y. Cui, J.F. Wang, C.M. Lieber, Nature 409 (2001) 66.
[3] Y. Lei, L.D. Zhang, G.W. Meng, G.H. Li, X.Y. Zhang, C.H. Liang, W. Chen, S.X. Wang, Appl. Phys. Lett. 78 (2001) 1125.
[4] Y.Q. Wang, G.Q. Hu, X.F. Duan, H.L. Sun, Q.K. Xue, Chem. Phys. Lett. 365 (2002) 427.
[5] H.Q. Cao, Y. Xu, J.M. Hong, H.B. Liu, G. Yin, B.L. Li, C.Y. Tie, Z. Xu, Adv. Mater. 13 (2001) 1393.
[6] H. Nakamura, Y. Matsui, J. Am. Chem. Soc. 117 (1995) 2651.
[7] G. Liu, F. Li, D.W. Wang, D.M. Tang, C. Liu, X.L. Ma, G.Q. Lu, H.M. Cheng, Nanotechnology 19 (2008) 025606.
[8] Z.B. Wu, F. Dong, W.R. Zhao, H.Q. Wang, Y. Liu, B.H. Guan, Nanotechnology 20 (2009) 235701.
[9] A.K. Alves, F.A. Berutti, F.J. Clemens, T. Graule, C.P. Bergmann, Mater. Res. Bull. 44 (2009) 312.
[10] T. Oota, I. Yamai, M. Yokoyama, J. Cryst. Growth 66 (1984) 262.
[11] D. Fabbri, F. Fabbri, G. Falini, V. Baravelli, A.A. Magnani, C. Torri, H. Maskrot, Y. Leconte, J. Anal. Appl. Pyrol. 82 (2008) 248.
[12] Y.C. Hong, J.H. Kim, C.U. Bang, H.S. Uhm, Phys. Plasmas 12 (2005) 114501.
[13] H.M. Zhang, P.R. Liu, X.L. Liu, S.Q. Zhang, X.D. Yao, T.C. An, R. Amal, H.J. Zhao, Langmuir 26 (2010) 11226.
[14] D.S. Dhawalea, D.P. Dubal, R.R. Salunkhe, T.P. Gujar, M.C. Rathb, C.D. Lokhande, J. Alloys Compd. 499 (2010) 63.
[15] Y. Zhang, Y. Gao, X.H. Xia, Q.R. Deng, M.L. Guo, L. Wan, G. Shao, Mater. Lett. 64 (2010) 1614.
[16] X.S. Zhou, F. Peng, H.J. Wang, H. Yu, J. Yang, J. Solid State Chem. 184 (2011) 134.
[17] P. Chen, W. Li, T.L. Zhou, Y.P. Jin, M.Y. Gu, J. Photochem. Photobiol. A: Chem. 168 (2004) 97.
[18] J.K. Burdett, T. Hughbanks, G.J. Miller, J.W. Richardson, J.V. Smith, J. Am. Chem. Soc. 109 (1987) 3639.
[19] R. Restori, D. Schwarzenbach, J.R. Schneider, Acta Crystallogr. Sect. B: Struct. Sci. 43 (1987) 251.
[20] T. Ohsaka, F. Izumi, Y. Fujiki, J. Raman Spectrosc. 7 (1978) 321.
[21] A. Chaves, K.S. Katiyan, S.P.S. Porto, Phys. Rev. B 10 (1974)3522 10 (1974).
[22] G. Liu, Y.N. Zhao, C.H. Sun, F. Li, G.Q. Lu, H.M. Cheng, Angew. Chem. Int. Ed. 47 (2008) 4516.
[23] G. Liu, C.H. Sun, L.N. Cheng, Y.G. Jin, H.F. Lu, L.Z. Wang, S.C. Smith, G.Q. Lu, H.M. Cheng, J. Phys. Chem. C 113 (2009) 12317.
[24] G. Liu, Z. Chen, C. Dong, Y. Zhao, F. Li, G.Q. Lu, H.M. Cheng, J. Phys. Chem. B 110 (2006) 20823.
[25] J. Hu, T.W. Odom, C.M. Lieber, Acc. Chem. Res. 32 (1999) 435.
[26] S. Sugai, H. Watanabe, T. Kioka, H. Miki, K. Kawasaki, Surf. Sci. 259 (1991) 109.
[27] D.R. Rainer, S.M. Vesecky, M. Koranne, W.S. Oh, D.W. Goodman, J. Catal. 167 (1997) 234.
[28] J.A. Rodriguez, T. Jirsak, J. Dvorak, S. Sambasivan, D. Fischer, J. Phys. Chem. B 104 (2000) 319.
[29] X.B. Chen, C. Burda, J. Phys. Chem. B 108 (2004) 15446.
[30] M.S. Wong, H.P. Chou, T.S. Yang, Thin Solid Films 494 (2006) 244.
[31] M. Sathish, B. Viswanathan, R.P. Viswanath, C.S. Gopinath, Chem. Mater. 17 (2005) 6349.
[32] F. Peng, L.F. Cai, H. Yu, H.J. Wang, J. Yang, J. Solid State Chem. 181 (2008) 130.